Project LiNaBioFluid

Deliverable D2.6: Publication of results on hydrodynamic modelling

Reporting period	from	**01.07.2016**	to	**30.06.2018**
Report completed and released		**27.03.2018**		

1. Objectives and Detailed Description

The goal of D2.6 concerns the publication of project results on hydrodynamic modelling, therefore, a summary of the knowledge gathered during the investigation in WP2 and a finalization of thoughts formulated during task 2.5 “Theoretical modelling”.

Task 2.5 hereby aimed at understanding of how the fluid transport on the bark bug cuticle is realized and how the underlying mechanism for micro- and nanostructured polymer and steel models can be utilized. First ideas towards this end have been previously stated within the internal WP 2 report, released on November 9th, 2017.

On December 29th, 2017, a manuscript with the title “The external scent efferent system of selected European true bugs (Heteroptera): a biomimetic inspiration for passive, unidirectional fluid transport” was submitted to the Journal of the Royal Society Interface. Containing an overview of the natural ante-type for the passive, unidirectional fluid transport (bug cuticle), the abstraction process and technical realization in different substrates (steel, polymers), different tested fluids (watery solutions, oils, cooling lubricants), and a conclusive chapter/supplement material about the physical model behind observed fluid behaviour, the manuscript was reviewed and revised on February 16th and February 28th and finally accepted for publication on March 8th.

The article was fully released as an open access (gold) article on March 28th/29th, 2018. All supporting data (e.g. supplement) is likewise freely accessible. The paper title is shown in Fig. 1.

Towards modelling, the paper follows a semi-analytical approach of fluid transport around structures with microstructured-shapes like those found in the external scent efferent system (ESES) of different European bugs (Fig. 2) and the abstracted, technical counterparts, as realized in Poly-Imide foils, polymers and steel.

INTERFACE

rsif.royalsocietypublishing.org

Research

Cite this article: Hischen F *et al*. 2018 The external scent efferent system of selected European true bugs (Heteroptera): a biomimetic inspiration for passive, unidirectional fluid transport. *J. R. Soc. Interface* 20170975.
http://dx.doi.org/10.1098/rsif.2017.0975

The external scent efferent system of selected European true bugs (Heteroptera): a biomimetic inspiration for passive, unidirectional fluid transport

Florian Hischen[1], Gerda Buchberger[1], Cristina Plamadeala[2], Oskar Armbruster[2], Ernst Heiss[4], Kai Winands[5], Martin Schwarz[6], Bert Jüttler[3], Johannes Heitz[2] and Werner Baumgartner[1]

[1]Institute for Biomedical Mechatronics, [2]Institute for Applied Physics, and [3]Institute for Applied Geometry, Johannes Kepler University Linz, Altenberger Straße 69, 4070 Linz, Austria
[4]Tiroler Landesmuseum, Josef-Schraffl-Straße 2a, 6020 Innsbruck, Austria
[5]Fraunhofer Institute for Production Technology IPT, Steinbachstraße 17, 52047 Aachen, Germany
[6]Oberösterreichisches Landesmuseum, Johann-Wilhelm-Klein-Straße 73, 4040 Linz, Austria

FH, 0000-0002-9280-0528; JH, 0000-0002-5608-5133

Figure 1: Title-screenshot of the journal article.

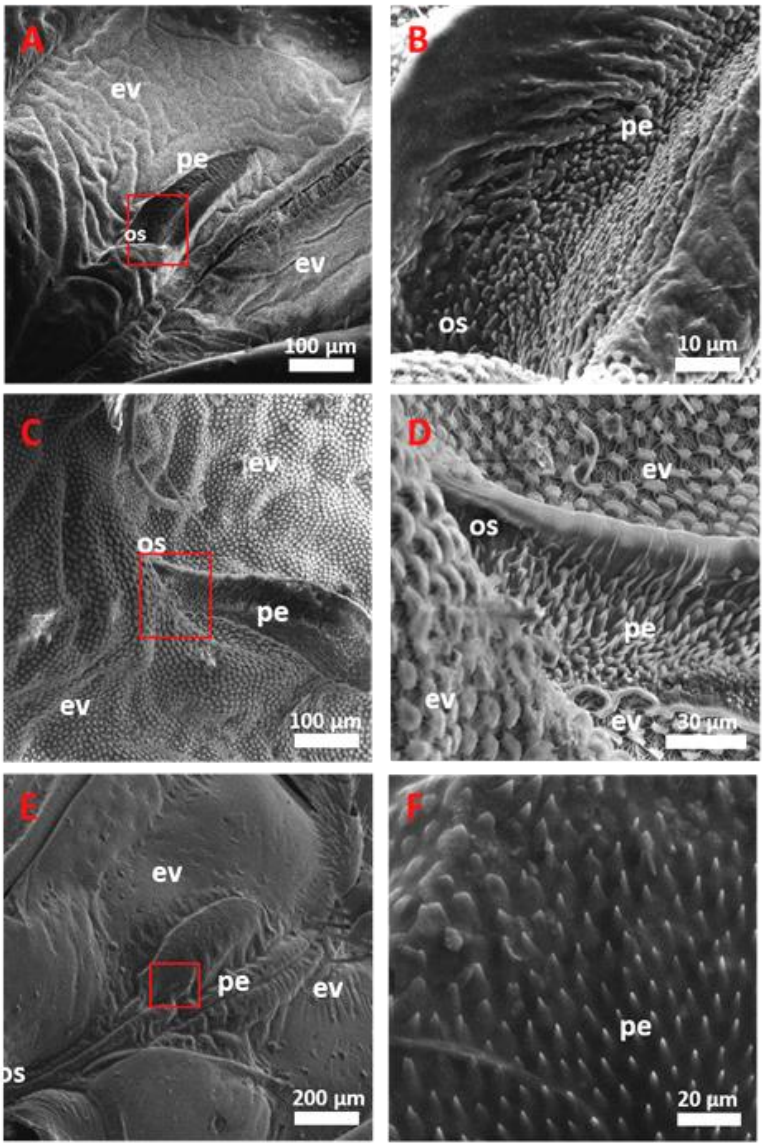

Figure 2: SEM overview of investigated species' ESES. Depicted parts of this system are the ostiole (os), the peritreme (pe) and the evaporioum (ev). **A** *Palomena prasina*. **B** Magnified box from A, showing a detail of the orientated microstructure of the peritreme close to the ostiole. **C** *Rhaphigatser nebulosa*. **D** Magnified box from C, again depicting the microstructure of the peritreme close to the ostiole. **E** *Tritomegas bicolor*. **F** Magnified box from E, showing a detail of the orientated microstructure of the peritreme. In this case the structure is located away farther from the ostiole than in A and C, closer located to the edge of the evaporium.

Geometries and structures, used as input for the model, follow the general morphology of the bug`s structures found in the ESES, meaning the resemble a drop like shape with different radii of curvature, as well as an inclined slope from base to top (see Fig. 3).

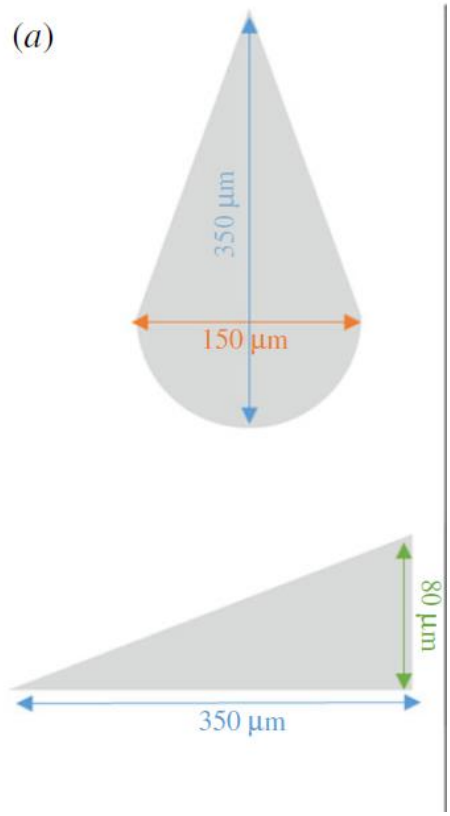

Figure 3: Abstracted geometry of modelled microstructures. Top: View from above → the drop like shape becomes apparent. Bottom: Cross section view, revealing the sloped inclination from base to tip. Depicted dimension are only exemplary (design of steel prototype), while for the model only ratios are of interest (e.g. length:width, or hight:width).

The physical model towards the explanation of investigated liquid transport, uses the approach of Laplace's equation (Laplace, 1805) for the pressure at a curved liquid surface (liquid meniscus):

$$p = \gamma \cdot \left(\frac{1}{r_1} + \frac{1}{r_2}\right) \quad (1)$$

with the pressure p, the surface tension γ and the principal radii of curvature r_1 and r_2, (the maximum and minimum values of the radius of the osculating circle. The directions of the normal plane where the radius takes its minimum and maximum are always perpendicular).
Here, we assume equilibrium and that the overall liquid pressure around a single unit cell (e.g. a single microstructure) is zero. This would be the case if the liquid were connected to an infinite liquid reservoir. In equilibrium, the liquid around a microstructure will form a so-called constant zero curvature surface if it fulfills:

$$\Delta p = 0 \Rightarrow H = 0 \Rightarrow \frac{1}{r_1} + \frac{1}{r_2} = 0 \quad (2)$$

with H being the local curvature. A comprehensive deduction of the physics behind the observed fluid transport can furthermore be found in the attached supplementary material.

The walls of each microstructure meet the bottom of the channel in a perpendicular way, hence for contact angles below 45° a capillary around each microstructure is formed. Assuming that the pressure around each structure is zero and the surface tension does not change, the surface of a liquid slug in the capillary around a single microstructure is

determined by the two main radii of curvature. Convex parts of the microstructure (tip and end) therefore “force” the liquid into expressing a concave radius of curvature in order to have pressure zero, hence holding the liquid front at close distance from the microstructure (Fig. 4 **A**), while straight parts of the microstructure (Fig. 4 **C**) allow for straight curvature of the liquid and therefore maximum distance of the liquid front from the microstructure. Consequently at transitioning zones of the structure (Fig. 4 **B**) there is a transitioning in liquid front distance from close to far and vice versa.

Following above approach it becomes obvious why our produced structures transported fluid unidirectional. PI foil prototypes as well as up-scaled replicas keep the liquid front at short distance at both curved ends of each individual microstructure while the liquid front is able to reach further out at the straight part in between. Hence, the liquid front is able to reach the next iteration of microstructures in forward direction (straight part faces a curved part), but not in backwards direction (curved part faces curved part), as also depicted in following Fig 5.
As long as there is fluid coming from a reservoir, this process of fluid surrounding an individual microstructure in the above-depicted way, reaching towards the next iteration of microstructures in forwards direction and so on, is repeated until the microstructured channel is filled or the reservoir is depleted. This also explains the always-observed v-shape in stop direction.

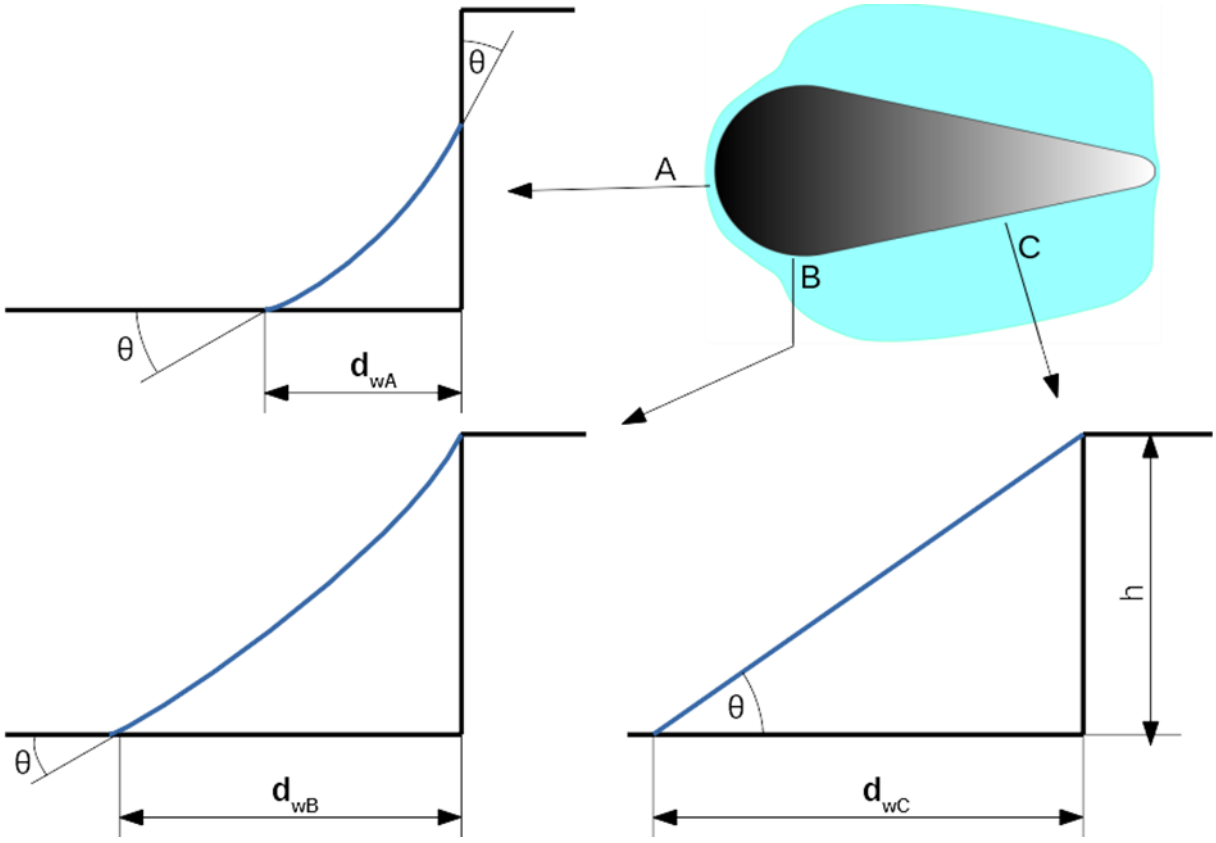

Figure 4: Distance of the waterfront calculated with regard to the main curvature of the microstructure at different zones (**A, B, C**). Θ is the contact angle, d_w the calculated distance with regard to the corresponding zone and *h* is the height of the structure.

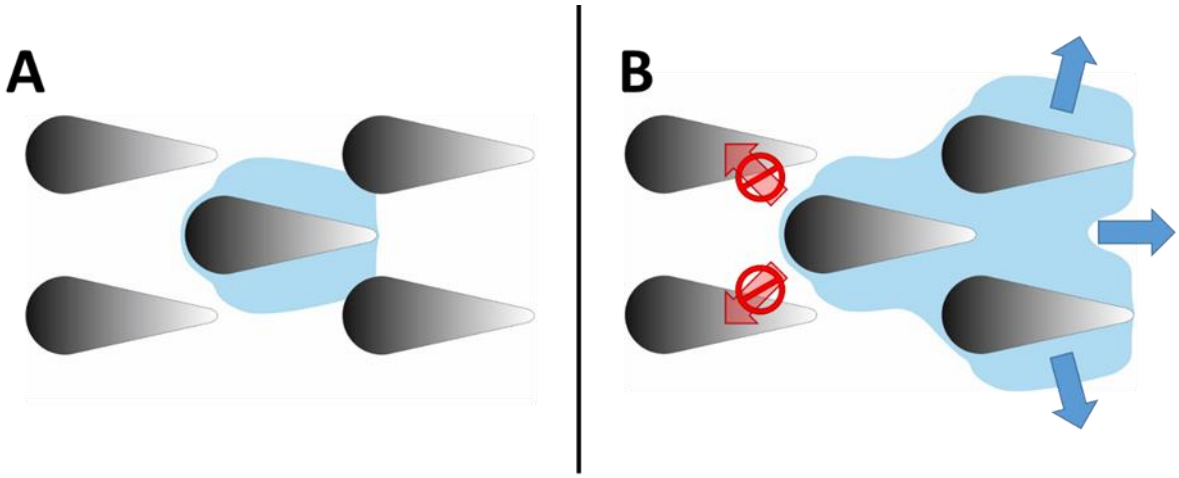

Figure 5: Schematic of the liquid slug around a single unit, reaching the next iteration of microstructures in forward direction. **A** A single unit cell surrounded by fluid as described in Figure 8. In direction of the microstructures` tip, fluid can reach the next iteration of microstructures, but not in direction of the base. **B** Newly reached structures are surrounded by fluid and forming a new fluid front. Fluid can jump from iteration to iteration in the forward direction but not in backwards direction, thus forming the observed v-shaped stopping front.

The model can be used as a starting point for simulation an optimization of drop like microstructures in even arrays, with regard to two main inputs: 1) Structure size and geometry (especially: main radii of curvature at base and tip, length of the straight part), and 2) the contact angle (needs to be <45° for a given liquid-surface combination). Varying these parameters will determine mainly how well the unidirectional aspect of the transport is covered (e.g. transport against gravity).

The influence of viscosity and surface tension can be accounted for, when looking at the analytical description of the dynamics of capillary liquid spreading in rectangular open channels as given by Berthier, Brakke & Berthier (2016). In an open rectangular channel with width *w* and height *h* the velocity of a liquid with viscosity η and surface tension γ, the velocity at penetration length *l* is given as

$$v = 2 \cdot \frac{\gamma}{\eta} \cdot \frac{h}{l} \cdot f_2 \qquad with\ f_2 = \frac{\left(\frac{w}{h} + 2\right) \cdot cos\theta - \frac{w}{h}}{\frac{12 \cdot w}{h} + \frac{24 \cdot h}{w}} \tag{1}$$

With identical geometry, i.e. with constant geometry factor f_2 and the same height and length, the liquid velocity is solely dependent on the ratio of surface tension and viscosity. For the shown approach, this means that the overall velocity of fluid transport is mainly depended from the chosen viscosity of the liquid and not so much from geometry of channels and structures.

2. Evaluation of Goals and Resulting Actions

The overall goal of D2.6 was successfully reached by m33 in form of the scientific article published in the Journal of the Royal Society Interface, as stated above, including a lot of the knowledge gained mainly throughout WP2, and especially during task 2.5.

The paper proves that the research in Tasks 2.3 until 2.5 was conducted fully in line with the work initially proposed in the GA and was fully achieved.

References:

Berthier, J., Brakke, K. A., & Berthier, E. (2016). *Open Microfluidics*. Hoboken, NJ, USA: John Wiley & Sons, Inc. https://doi.org/10.1002/9781118720936

Hischen, F. et al. (2018) The external scent efferent system of selected European true bugs (Heteroptera): a biomimetic inspiration for passive, unidirectional fluid transport. J. R. Soc.Interface 20170975. http://dx.doi.org/10.1098/rsif.2017.0975

Laplace, P. S. (1805). An essay on the cohesion of fluids. *Philosophical Transactions of the Royal Society of London*, *95*, 65–87.

Supplementary Material:

Flow around structures: An equilibrium approximation

The structures that protrude from the surface can be described as general cylinders which is defined as a surface consisting of all the points on all the lines which are parallel to a given line and which pass through a fixed plane curve in a plane not parallel to the given line. In our case the droplet-shaped footprint is the fixed planar curve and the parallel lines defining the cylinder are perpendicular to the surface of this footprint. These general cylinders are truncated at a given height above the surface.
If now liquid is brought in contact with such a general cylinder and the base surface respectively, the liquid surface will form in such a way that the energy of the system is minimized. The surface of the liquid can be described by a function *f(x,y)* over the surface plane, where x and y are the planar coordinates. For a general function *f(x,y)* the local curvature *H* is defined as

$$H=-\frac{1}{2}\cdot\nabla\cdot\left(\frac{\nabla F}{\|\nabla F\|_2}\right)=\frac{\left[1+\left(\frac{\partial f}{\partial x}\right)^2\right]\frac{\partial^2 f}{\partial y^2}-2\cdot\frac{\partial f}{\partial x}\cdot\frac{\partial f}{\partial y}\cdot\frac{\partial^2 f}{\partial x\partial y}+\left[1+\left(\frac{\partial f}{\partial y}\right)^2\right]\frac{\partial^2 f}{\partial x^2}}{2\cdot\sqrt{\left[1+\left(\frac{\partial f}{\partial x}\right)^2+\left(\frac{\partial f}{\partial y}\right)^2\right]^3}} \quad (1)$$

which is connected to the Laplace-pressure of the liquid as

$$\Delta p=\frac{\partial E}{\partial V}=\gamma\cdot\left(\frac{1}{r_1}+\frac{1}{r_2}\right)=2\cdot\gamma\cdot H \quad (2)$$

where r_1 and r_2 are the main radii of curvature. If the liquid is connected to an infinite liquid reservoir at pressure 0, then the liquid surface will form a so called constant zero curvature surface, also called minimal surface with fulfils

$$\Delta p=0 \;\Rightarrow\; H=0 \;\Rightarrow\; \frac{1}{r_1}+\frac{1}{r_2}=0 \quad (3)$$

If the contact angle of the liquid-solid combination is below 45°, energetically stable liquid surfaces can be found, that fulfil the above condition. In general it is hard to find minimal surfaces based on arbitrary boundary conditions. In our case the boundary conditions is the contact angle at which the liquid interacts with the solid surface.

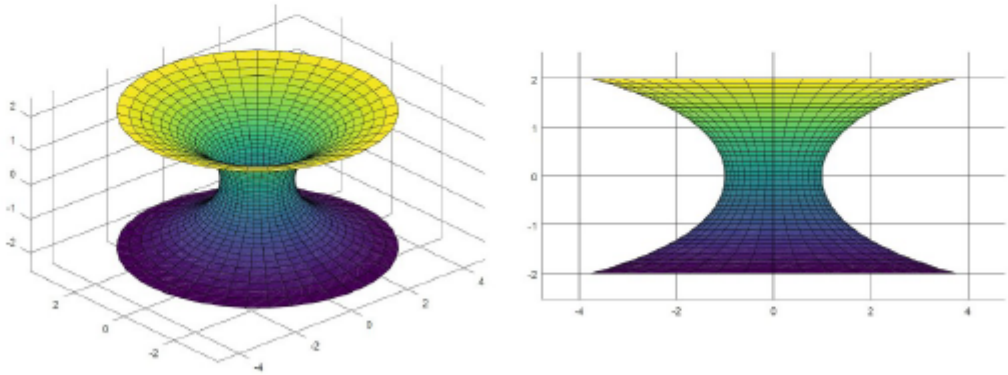

Figure S1: Part of a catenoid with center axis in y-direction at x=0 and z=0 with radius a=1 at bird's eye view (left) and side view (right).

In the case of a right circular cylinder (curve in the plane is a circle), a simple solution for the minimal surface problem given the contact angle can be found to be a catenoid. A catenoid is a surface arising by rotating a catenary curve about an axis. The catenoid may be defined by the following parametric equations:

$$x = a \cdot \cosh\frac{v}{a} \cdot \cos u \quad y = a \cdot \cosh\frac{v}{a} \cdot \sin u \quad z = v \tag{4}$$

here $u \in [-\pi, \pi[$, $v \in \mathbb{R}$ and a is a non-zero real constant which is the radius of curvature of the catenary curve at the vertex as well as the radius for the rotation of the vertex around the z-axis.
In figure S1 a catenoid can be seen in two views with a=1. Clearly the catenoid has a constant mean curvature of zero.
Now for the right circular cylinder of finite height h we have to distinguish two cases. The first one is depicted in Figure S2.

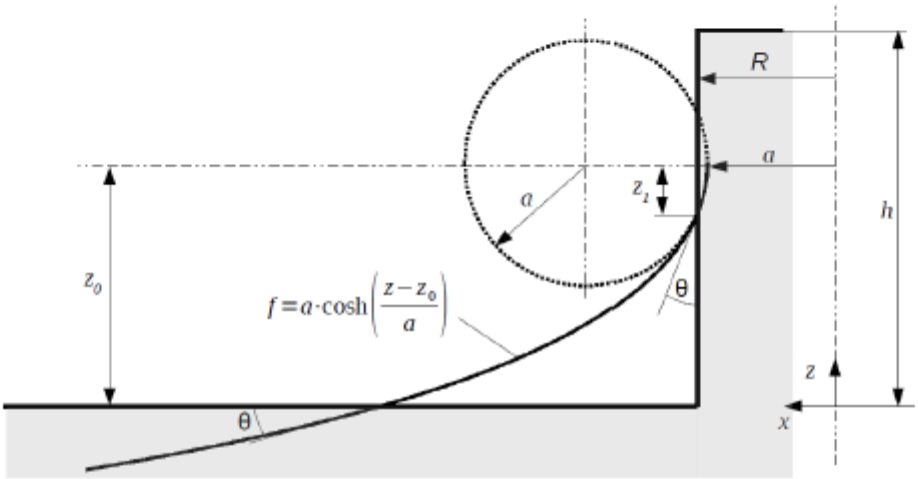

Figure S2: Case one for a catenary curve *f(z)* forming a catenoid when rotating around the z-axis. A right circular cylinder with radius R as well as the base surface are intersected at an angle θ, the contact angle.

Here the catenoid with vertex radius of curvature a intersects with the cylinder as well as with the surface, i.e. the xy-plane. Now the radius of the cylinder R and the contact angle θ are given and the parameter (radius) a of the catenary curve and the z-position of the vertex z_0 as well as the distance to the intersection z_1 have to be determined. For this we need the fact that

$$\frac{df}{dz} = \sinh\left(\frac{z - z_0}{a}\right) \tag{5}$$

Applying this at the intersection of catenoid and cylinder, i.e. at a distance z_1 from the vertex yields

$$z_1: \quad \sinh\left(\frac{y_1}{a}\right) = \tan\theta \quad \Rightarrow \quad z_1 = a \cdot \operatorname{arcsinh}(\tan\theta) \tag{6}$$

At the intersection of catenoid and cylinder the function f equals the cylinder radius R, i.e. $R = a \cdot \cosh(z_1/a)$ thus by inserting z_1 from Eq. 6 we obtain the analytical solution

$$a = \frac{R}{\cosh\left[\operatorname{arcsinh}\left(\tan\theta\right)\right]} \tag{7}$$

Now the position z_0 of the vertex can be found

$$\sinh\left(\frac{z_0}{a}\right) = \cot\left(\theta\right) \quad \Rightarrow \quad y_0 = a \cdot \operatorname{arcsinh}\left[\cot\left(\theta\right)\right] \tag{8}$$

These relationships derived so far hold true if the height of the cylinder is larger than the z-position of the vertex, i.e. if $h > z_0$. If this is true, then the above derived iteration in Eq. 7 converges and real solutions for a and z_0 can be found. A solution for the catenoid forming the liquid surface around a cylinder of radius 1.1 is shown in Figure S3.

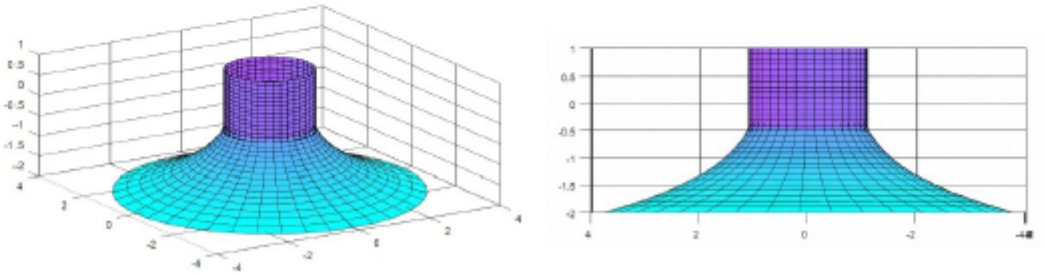

Figure S3: Liquid surface (blue) formed around a cylinder (violet) of radius 1.1 in bird's eye view (left) and side view (right).

If the radius of the cylinder R is too large or the height h is too low, another solution has to be found. The principle is depicted in Figure S4.

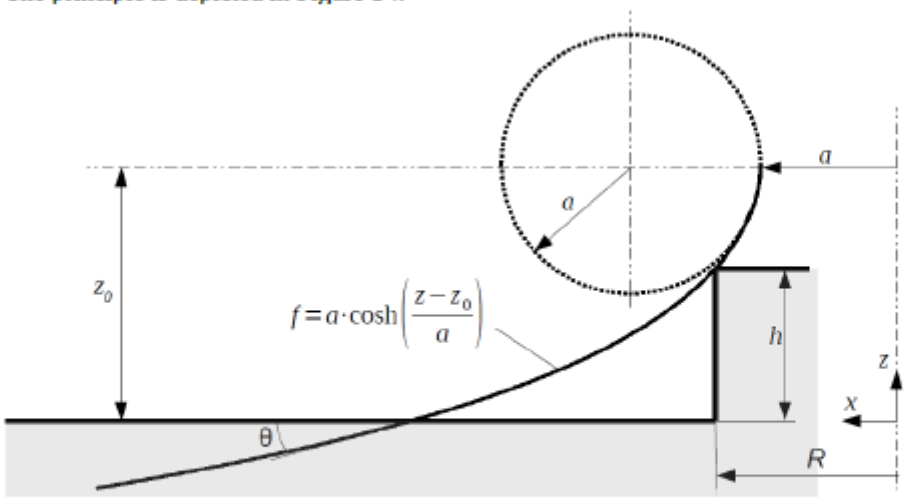

Figure S4: Case two for a catenary curve *f(z)* forming a catenoid when rotating around the z-axis. The base surface is intersected at the contact angle θ. The upper edge of the cylinder forms a singularity, i.e. it is part of the catenary curve.

Here the edge of the cylinder, i.e. the position $(x,z)=(R,h)$ is located on the catenary curve, thus we find

$$R = a \cdot \cosh\left(\frac{y_0 - h}{a}\right) \tag{9}$$

In the current case Eq. 8 is also valid. Combining Eq. 8 and Eq. 9 we obtained

$$a = R \cdot \cosh\left\{\frac{a \cdot \sinh[\cot(\theta)] - h}{a}\right\}^{-1} \tag{10}$$

This implicit equation for a given R and θ can simply be solved by iteration with a start value for a to be set to R. Typically we reach convergence to a precision of <1% after 3 to 10 iterations for $25° < \theta < 44°$ and $R > 0$.
The calculation of the z-position of the vertex can be done according to Eq. 8.

This second case where the liquid meniscus hits the upper edge of the structure at $z=h$ contains the special case that $R \to \infty$, i.e. that the structure has a straight wall. However, this case is rather simple to treat as the solution is a plane that intersects the bottom at the contact angle θ and that hits the upper edge of the structure. This corresponds to case C in Figure 8 of the manuscript.

Now in order to find the average mean zero curvature surface the liquid forms around a general cylinder with a more or less arbitrary footprint, we used the following approximation: If the footprint (in our case the droplet-shape) exhibits no absolutely abrupt changes in the curvature, i.e. if it is at least twice continuously differentiable, the surface is locally approximated by a cylinder with the radius of the local radius of curvature of the footprint. For this cylinder the intersection of the corresponding catenoid with the xy-plane is calculated. The intersection of the catenary curve in the plane perpendicular to the tangent plane on the general cylinder is found. This point is marked. The procedure is repeated for a finite set of points along the footprint of the structure. Finally the found points are interpolated. Thus we approximate the structure locally by cylinders and smoother the catenoid-surfaces in order to find a good approximation for the minimal surface surrounding the general cylinder.
This can be done for rather general footprints as long as the curvature changes moderately along the outline. Either the shape is given locally by analytic functions (biarcs, splines, hyperbolas, …) from which the local curvature can be directly derived, or the footprint is given by a set of xy-coordinates of supporting-points. From these the local curvatures and the tangent planes can be estimated numerically.

This was done for the droplet-shaped structures of the bark bugs as shown in Figure 7 and 8 of the main manuscript. There the intersection point of the catenoid with the xy-plane, i.e. f(z=0) is shown for the given structure, indicating the asymmetric fluid behaviour.